Comparison of Thermography Techniques for Inspection of F/A-18 Honeycomb Structures

Marc Genest[*], Clemente Ibarra-Castanedo[†], Jean-Marc Piau[†], Stéphane Guibert[†], Mirela Susa[†], Abdelhakim Bendada[†], Xavier Maldague[†], Micheal Brothers[*], Abbas Fahr[*]

[*] *National Research Council Canada, Institute for Aerospace Research, 1200 Montreal Road, Ottawa, Ontario, Canada, K1A 0R6*

[†]*Computer Vision and Systems Laboratory, Department of Electrical and Computer Engineering, Université Laval, Quebec City, Quebec, Canada, G1K 7P4*

Abstract

CF-18 aircraft have been in service in the Canadian Forces (CF) for over 20 years. Over the lifetime of these aircraft, some of the flight control surfaces, such as rudders and flaps, that are made of honeycomb sandwich structures, are subjected to water ingress or impact damage that sometimes lead to delamination and disbond of the facesheets (skin). In the CF, the current practice for detection of water ingress in flight control surfaces uses a passive thermography technique. Generally, the inspections of installed flight control surfaces for water ingress are performed during the winter where aircraft can easily be cold-soaked outdoor. The water heat capacitance is used to create thermal gradients when aircraft slowly warm-up inside a heated hangar. Even though this technique is successful for detection of water ingress, its sensitivity and resolution are not optimal and the presence of disbond and delamination are not necessarily detected. This paper presents comparisons between passive and different active thermography techniques applied for nondestructive inspection (NDI) of honeycomb structures with simulated flaws as found in flight control surfaces of CF-18 aircraft. The results are shown for reference specimens and for real rudders. It is demonstrated that active thermography techniques (ATT) are more sensitive and provide a better spatial resolution than passive thermography. In addition, unlike the passive thermography that requires cold-soaking of the aircraft for a few hours, active thermography can be carried out in a shorter time thus reducing the aircraft downtime. The results from ATT are also compared to those of the conventional ultrasonic C-scan method.

1 Introduction

The CF's investigation into emerging nondestructive technologies to find a more suitable technique for inspecting its CF-18 flight control surfaces began in late 1995, when it was decided to send the CF-18 with the highest flight-hours to McClellan Air Force Base (AFB) in Sacramento, California for NDI by both neutron radiography and X-radiography. While the CF had been using X-radiography inspections since the aircraft had been introduced into service[1], the McClellan AFB facility was the first Canadian use of the emerging technology of neutron radiography.

The inspection results indicated the presence of water and corrosion in the flight control surfaces inspected. These inspections revealed indications of water ingress in the graphite/epoxy skin layers and in the aluminum honeycomb core structure of the port rudder, as well as the possibility of corrosion in the core.[2] In addition, neutron radiography inspections revealed a total of 93 anomalies, including moisture, cell corrosion, damaged honeycomb core, foreign object material, voids, and repaired areas.[3]

Rudders are flight control surfaces usually attached to the vertical stabiliser of aircraft, which allow controlling the yaw in the horizontal axis.[4] Figure 1 presents the location of rudders on a CF-18 aircraft as well as an example of the results of an in-flight disintegrated rudder that lead to intensive investigation for improving NDI method for detection of water ingress and disbond. After the CF-18 returned to Canada, a rudder was removed from the aircraft and put through a rigorous NDI program, including x-radiography (film and real-time), ultrasonics through transmission and pulse-echo, infrared thermography, and neutron radiography. Typical results obtained by these techniques can be found in Ref. 4. Of all the techniques investigated, only through transmission ultrasonics and neutron radiography were successful in identifying large areas of hydration, and only neutron radiography could identify the small areas of moisture entrapment and hydration.[6] At the end of the NDI trials, the rudder was disassembled and the levels of moisture entrapment were determined. All areas of moisture entrapment and hydration found during the destructive testing were the same areas that had been detected using neutron radiography.[6]

During these investigations the thermography techniques investigated were not the optimal methods and newer thermography techniques such as lock-in thermography and vibrothermography were not assessed. Also, powerful data processing technique were left out.

In this paper, the thermography techniques previously assessed and newer techniques developed for NDI of honeycomb sandwich structures are compared. In addition, the thermography results are compared to those of ultrasonic c-scan. The NRC-IAR has previously demonstrated the feasibility of pulsed thermography to detect defects in honeycomb structures[7, 8]. This study assesses the most common thermography techniques: passive, pulsed, pulsed phase, lock-in and vibro compared to the passive thermography used by the Canadian Forces (CF) for detection of water ingress in its CF-18 rudders.[9] The inspections were carried out on two reference panels manufactured by the NRC-IAR and two rudders from a CF and a US Navy (USN) aircraft.

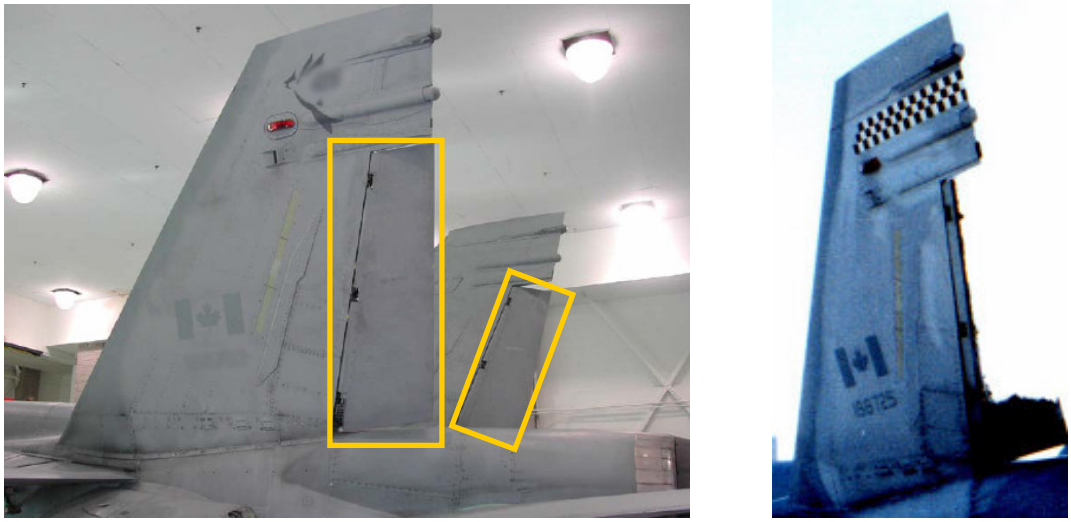

(a) (b)

Figure 1 a) A photograph of installed rudders on a CF-18 aircraft. b) A photograph of a CF-18 rudder lost during a training mission.

The following sections discuss briefly the theory of the diverse thermography inspection techniques assessed. Then, a description of the reference honeycomb panels manufactured and the experimental setup of the NDE techniques used is provided. Subsequently, inspection results of the reference panels and of the rudders are presented and discussed.

2 Thermography

In thermographic NDI[10], part of the infrared (IR) band of the electromagnetic spectrum is used to map the surface temperature of an inspected item. In general, a source of energy is used to create a temperature difference between the specimen and the surrounding environment. As the specimen returns to thermal equilibrium, the heat flow is monitored using an IR imaging device (typically an IR camera) and the temperature evolution is recorded in a sequence of thermal images. Variations in the structure or material properties result in variations in heat flow and surface temperature.

2.1 Passive Thermography

In passive thermography, heat transfers that occur in normal use of structure or equipment are monitored and used to detect anomalies. Problems or abnormalities in the inspected item usually result in unusual temperature profiles. Thus, without the need of external heat source an IR camera can be used to map the surface temperature and diagnose problems. Examples of successful used of passive thermography include monitoring of over heating of engines and electrical circuits, moisture detection, building insulation inspection, etc.

2.2 Pulsed Thermography

In pulsed thermography (PT), energy is applied to the specimen using a pulsed excitation, whose duration varies from a few milliseconds for good thermal conductors to a few seconds for low-conductivity materials. When a thermal wave intersects an interface from a layer of high conductivity to a layer of lower conductivity, like in the

case of delamination or disbond; the cooling rate is locally delayed resulting in an accumulation of energy above the surface that can be detected by an IR camera. Thus, defective areas can be distinguished from sound areas.

A gross estimation of the flaw depth can be made using the thermal propagation time (t) that depends on the thickness of the material (z) and of its thermal diffusivity (α):

$$t \approx \frac{z^2}{\alpha} \tag{1}$$

Where α is defined by $k / (c \cdot \rho)$ and k is the thermal conductivity, c is the specific heat and ρ is the density. Equation 1 is one-dimensional approximation and requires knowledge of the thermal properties of the item under inspection. In complex structures, it is usually more practical to use calibration specimens to estimate the depth location of the flaws.

2.2.1 Pulsed Phase Thermography

Pulsed phase thermography (PPT) is a powerful add-on to the regular pulsed thermography. PPT is a processing method in which the thermal images are transformed from the time domain to the frequency domain.[11] This can be performed by processing a thermogram sequence with discrete Fourier transform (DFT):

$$F_n = \sum_{k=0}^{N-1} T(k) e^{-2\pi i k n / N} = \mathrm{Re}_n + i\,\mathrm{Im}_n \tag{2}$$

Where n designates the frequency increments (n=0,1,…N-1), and Re and Im are the real and the imaginary parts of the DFT, respectively. For convenience, a computationally efficient algorithm, known as fast Fourier transform (FFT) is generally used to calculate the DFT. Once the data has been converted to the Fourier domain, the phase (ϕ) and amplitude (A) image of the different frequencies can be calculated using:

$$A_n = \sqrt{\mathrm{Re}_n^{\,2} + \mathrm{Im}_n^{\,2}} \qquad \text{and} \qquad \phi_n = tan^{-1}\left(\frac{\mathrm{Im}_n}{\mathrm{Re}_n}\right) \tag{3}$$

The phase is particularly advantageous since it is less affected by environmental reflections, emissivity variations, non-uniform heating, surface geometry and orientation. The phase characteristics are very attractive not only for qualitative inspections but also for quantitative ones.[12,13]

PPT can be compared to lock-in thermography (discussed later) since both techniques provide phase information. However, PPT is faster than lock-in thermography (LT) since the latter is a mono-frequency test. On the other hand, PPT inspections contain several frequencies simultaneously. Thus, for a single experiment the frequency content of the transient energy excitation, such as PT, is richer than that of a steady regime, such as lock-in thermography.

2.2.2 Thermographic Signal Reconstruction (TSR)

Thermographic signal reconstruction (TSR)[14] is a processing technique that allows increasing spatial and temporal resolution of a thermogram sequence, while reducing the amount of data to be analysed. TSR is based on the assumption that temperature profiles for non-defective areas should follow the decay curve given by the one-dimensional solution of the Fourier diffusion equation for an ideal pulse uniformly applied to the surface (z=0) of a semi-infinite body, which may be written as follows:[15]

$$T(t) = \frac{Q}{e\sqrt{\pi \cdot t}} \tag{4}$$

Where $T(t)$ is the temperature evolution, Q is the energy injected at the surface and e is the thermal effusivity of the sample defined as: $e = \sqrt{k\rho c}$. Equation 4 may be rewritten in a logarithmic notation and expanded into a polynomial series:[16]

$$\ln(\Delta T) = \ln\left(\frac{Q}{e}\right) - \frac{1}{2}\ln(\pi t) = a_0 + a_1 ln(t) + a_2 ln^2(t) + \ldots + a_n ln^n(t) \tag{5}$$

The noise reduction by polynomial interpolation (TSR)[17,18] makes possible the use of derivative processing to enhance the visibility of the defects. The first and second derivatives of the thermogram sequence provide information on the rate of temperature variation. These measurements can be compared by analogy to the relations between position, velocity and acceleration in mechanics. The raw data from thermograms corresponds to the surface temperature of the inspected object (position). The first derivative gives information on the rate of the

surface temperature variation (velocity), and the second derivative provides information on the acceleration or deceleration of the surface temperature variation (acceleration).

2.3 Lock-In Thermography

In lock-in thermography (LT), the energy is supplied to the specimen using a periodical excitation and is based on monitoring the time dependence between the excitation signal and the specimen response. The duration of the excitation, which varies from a few seconds to a few minutes, depends on the material properties and thickness of the inspected item. The excitation sources usually employed in LT are heating lamps or laser beam.

The depth (μ) reached by a sinusoidal thermal wave that penetrates into a sample material depends on the excitation frequency, the material properties and the pulsation of the excitation source (ω) according to the thermal diffusion length:

$$\mu = \sqrt{\frac{2 \cdot \alpha}{\omega}} \tag{6}$$

Once a steady-state has been reached, the reconstruction of a thermal wave signal can be achieved by using the measurement of the specimen surface temperature in response to the applied excitation. The variation of amplitude and phase between the reconstructed specimen response and the excitation signal is then used to identify the flaws. Several methods can be applied to compute the amplitude and phase variations, including standard lock-in method, Fourier transform, four-point (4-bucket) algorithm[19], etc.

2.4 Vibrothermography

Vibrothermography (VT), also called thermosonic, is a method based on the conversion of mechanical to thermal energy. In VT, ultrasonic waves are used as source of mechanical energy and are introduced into a specimen to generate heat at flaw locations. The nature of the heat generated results from friction of the rubbing crack surfaces, clapping and plastic deformation. The heat generated is affected by both the frequency and the amplitude of the excitation signal.[20] Therefore, the duration of the experiment depends on the number of frequencies tried. In order to generate heat, the flaws must be excited in a proper resonance mode. Both frequency sweep and random excitation can be used to excite the structure. Special care must be taken to ensure that the mechanical excitation applied to the structure will not increase the size of the damage or induce new damage into the structure. To reduce this risk, low power excitation combined with proper frequencies must be used.

One of the main differences between vibrothermography and other thermography methods resides in the heat source. As seen in Figure 2, while in optical thermography methods the heat source is external to the sample, such as a laser or heating lamps, in VT the source of heat is the flaw itself; thus, eliminating the effect of non-uniform heating.

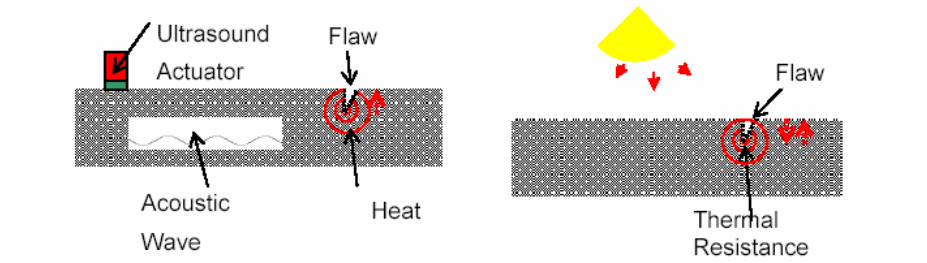

Figure 2 Comparison between vibrothermography and optical thermography method.

The main disadvantage of VT is that contact or coupling between the source and the sample is required. The coupling is the change of medium between the ultrasound source and the sample. It is recommended that a coupling material be placed between the ultrasonic horn and the sample for two reasons. First, to match the impedance between the horn and the sample, thus improving the efficiency of the source by maximising the power transmitted, limiting losses, and eliminating unwanted heat in the vicinity of the ultrasound injection point. Secondly, since the energy source acts like a hammer, hitting the surface of the sample at high frequency, a good coupling will avoid inducing damage into the samples. The pressure used to hold the horn against the sample also affects the coupling and has a great impact on the thermal response.[21]

3 Specimens

To demonstrate the capabilities of the different thermography techniques described on known defects, two honeycomb sandwich reference panels were manufactured. The face sheets of the reference panels were made

following the standard CF rudder facesheet (skin) thickness and orientation. However, they were manufactured using two variants of aluminium honeycomb core. One is 15.875mm (0.625”) thick and is made of larger cell size (3/16”) (lower core density), while the other core used is 50mm (1.9685”) thick and has smaller cell size (1/8”) (higher core density). A schematic of a manufactured panel showing the Teflon insert location is presented in Figure 3. A photograph of the two rudders used in the study is presented in Figure 4a (gray → CF, brown → USN).

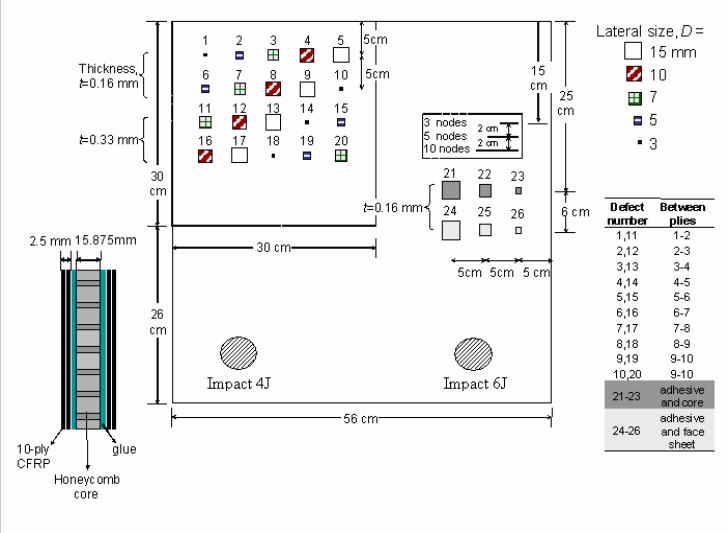

Figure 3 A schematic of a manufactured panel containing flaws.

4 Experimental Setup

4.1 Passive Thermography

Passive thermography experiments were carried out according to the CF procedure[9], except that it was performed during daytime. The rudders and a calibration panel were cold-soaked for at least three hours. The outside winter weather (-12ºC or 10.4F) conditions were adequate to perform the procedure in Ottawa. Figure 4 shows photographs of the coupons during the cold-soaking phase.

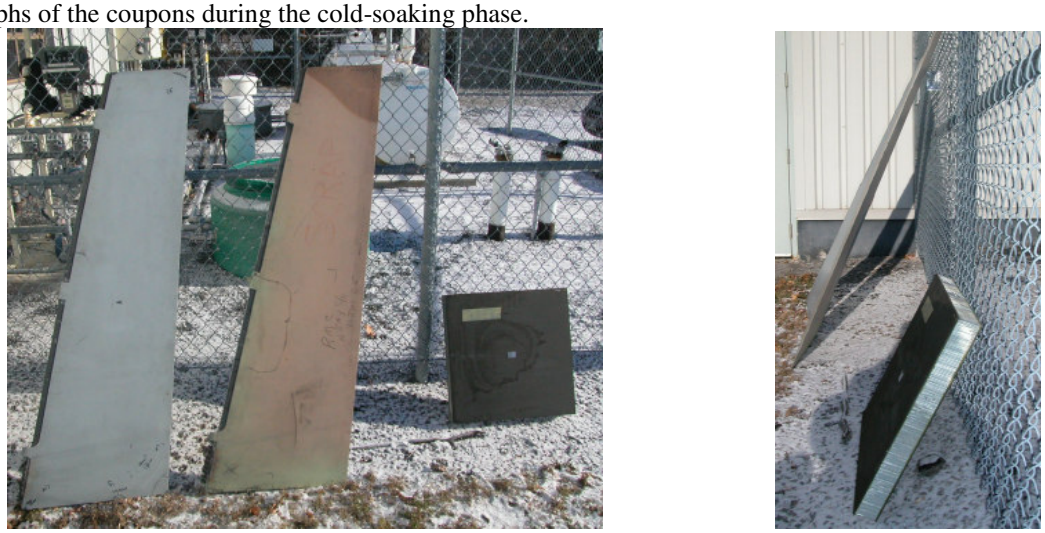

(a) (b)

Figure 4 A photograph that shows (a) natural cold soaking of rudders and a calibration panel; (b) the angle used while cold soaking the rudders and calibration panel.

4.2 Pulsed Thermography

The pulsed thermography inspections were performed by both the NRC-IAR and the UL. The NRC-IAR performed the inspection by using a ThermaCAM® SC3000 infrared (IR) camera, designed by Flir Systems, that was used to monitor the evolution of the surface temperature, which is part of a commercial thermography system

designed by Thermal Wave Imaging Inc. While the UL used a Phoenix IR camera also designed by Flir Systems using a homemade PT system.

4.3 Lock-in Thermography

The heat sources used for the lock-in thermography experiments are regular stage halogen lamps. The equipment can operate with up to six halogen lamps mounted on a frame. The frame gives flexibility in the setup since it allows repositioning and rotation of the lamps. Each lamp is independently controlled by a dimmer that can regulate the lamp intensity by increments of 1%. With the 1000W lamps used, the smallest intensity increment is 45µW/mm^2. The acquisition frame rate used depends on the period of the modulated thermal source and was set at 100 frames per thermal wave source period.

4.4 Vibrothermography

The vibration device used by the UL for vibrothermography experiments is an ultrasonic plastic welder with a frequency of 20 kHz and a maximum power of 2200W. For the experiments, 75% (1650W) of the power was used. However, this is not the power sent into the material. The real power introduced into the material depends on the elastic impedance match between the transducer horn, the coupling agent and the inspected material. By increasing the matching impedance between the horn and the material, it is possible to augment the power transmitted into the sample. In the vibrothermography experiments carried out, the best impedance coupling achieved was about 20%. Therefore, it is more realistic to think that around only 300W were injected into the inspected structures. For the results reported in this document, the inspection parameters used are: holding pressure 250 PSI, excitation duration between 250ms and 2000ms, acquisition of 300 frames at 88Hz. Photographs of typical vibrothermography setup are shown below.

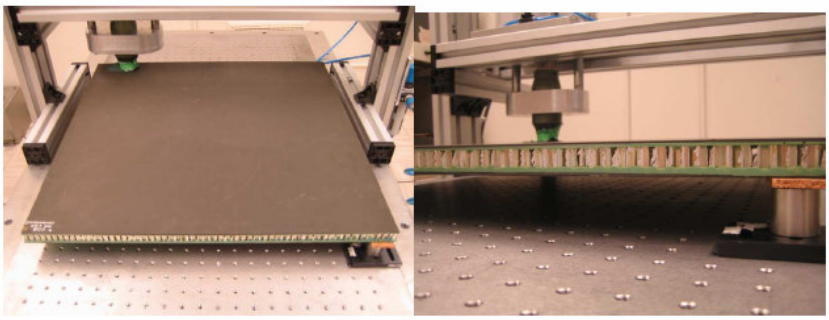

(a) (b)

Figure 5 Photographs of the setup used in vibrothermography.

5 Results

5.1 Ultrasonic

This section presents ultrasonic (UT) results and since UT is the most commonly used NDI technique, it is used as a reference. Through transmission inspection techniques interrogate the structure through the whole thickness. This means that flaws, anomalies and features detected are either in the top facesheet, the bottom facesheet or somewhere in between. Through transmission UT c-scan results (Figure 6) show an anomaly in both CF and USN rudders next to the middle hinge (anomaly A). None of the other through transmission techniques tried (Neutron- and X- radiography) shows this anomaly. Thus, this anomaly is not the indication of the presence of water in the rudder.

All of the through transmission techniques tried show the metallic reinforcement structure, the titanium channel at the leading edge, the foam filler, and both the leading and the trailing edges.

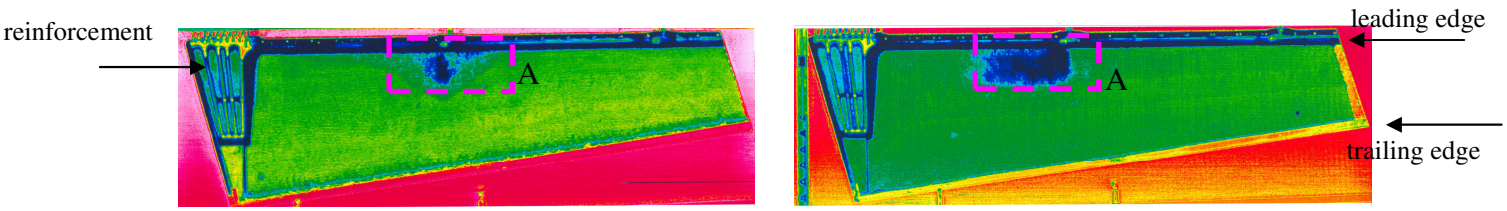

Figure 6 CF and USN rudder through transmission UT c-scan inspection results, provided by Quality Engineering Test Establishment (QETE).

In pulse-echo mode, as opposed to through transmission, access to only one side of the structure is required. A pulse-echo ultrasonic c-scan inspection result of a reference panel is shown in Figure 7a. As seen, all the Teflon inserts simulating delamination and disbond were detected as well as the two impact damage sites. Simulated node bond failures (node separation) were not detected. Since the UT inspection was performed from the top face sheet while the panel was sitting on its bottom face sheet; the injected water, which was on the bottom face sheet at the time of the inspection, was not detected. The blue circle shape feature in the center of the image is likely the consequence of non-uniform resin thickness resulting from the vacuum applied during the curing process. The UT pulse-echo inspection results of the F/A-18 rudder are similar to those obtained in through transmission with a few additional features detected (example provided in Figure 7b)

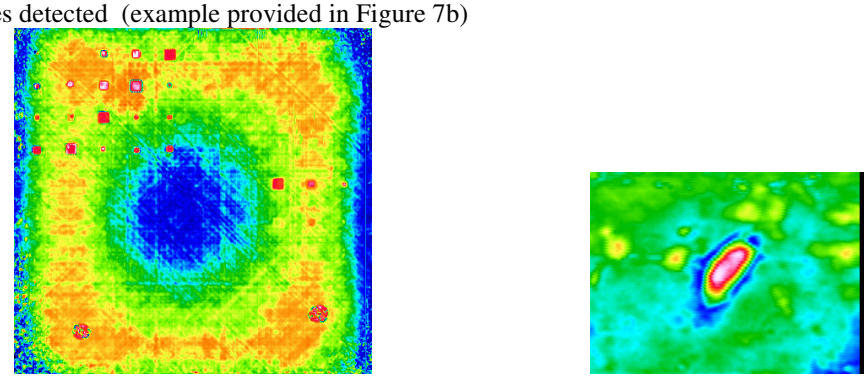

(a) (b)

Figure 7 Ultrasonic pulse-echo c-scan inspection result of (a) a reference panel; (b) an additional feature detected on CF rudder.

5.2 Passive Thermography

Only a few of the simulated delaminations were successfully detected by the passive thermography inspections (Figure 8a). Two reasons may explain why the water was not detected. First, the amount of water present might have been too little and second, the angle used during the cold-soaking process might have been too steep for the amount of water present. No anomalies were detected in the rudder in passive thermography inspections (Figure 8b). Only the hinges and the metallic reinforcement of the rudders were visible.

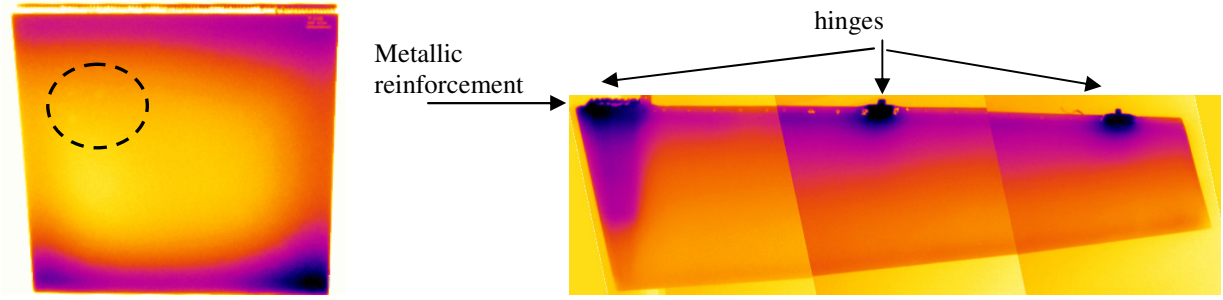

(a) (b)

Figure 8 Passive thermography inspection results of a reference panel (a) top face sheet; (b) Passive thermography results (CF rudder port side).

5.3 Pulsed and Pulsed Phase Thermography

As seen in Figures 9 and 10, the results obtained by PT and PPT are comparable: all Teflon inserts except the smallest single layer located between face sheet ply 9 and 10 were detected. The simulated face sheet disbonds (both skin to adhesive and adhesive to core) were all detected, but at a later time sequence; while the simulated node bond failures were not detected and the two impact damage sites were clearly detected. The main difference between the NRC-IAR and the UL results is in the contrast obtained and that can be explained by two factors. First, the field of view used at the NRC-IAR gives a higher spatial resolution, thus smaller defects are easier to see. Second, the amount of energy injected in the part and the distance between the flash lamps and the part was significantly different. Nevertheless, both results show that PT and PPT are suitable for the detection of delamination and both artificial and real disbonded areas.

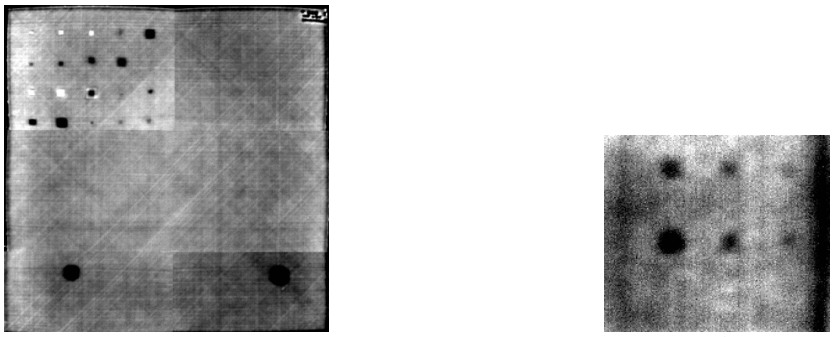

(a) (b)

Figure 9 PT inspection results (a) first derivative of a reference panel at t=0.735s; (b) first derivative of the simulated disbond areas at t=8.751s.

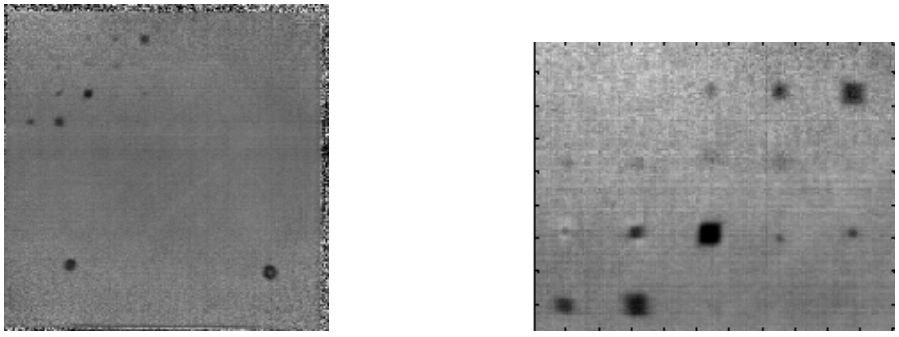

(a) (b)

Figure 10 PTT inspection results of a reference panel (a) synthetic phase at f = 0.82 Hz for the specimen (b) phase a f=0.08Hz. A 7th degree polynomial was used for TSR.

The manufactured panels were also inspected for the presence of water. In this setup, the panels were positioned horizontally such that the water was in contact with the bottom face sheet. PT was then carried out from the bottom face sheet and as shown in the table and figure below, amount of water as small as 0.02 ml, corresponding to approximately 10% of the full cell, were detected in each panel, respectively.

Table 1 Amount of water per cell*

0.25	0.22	0.2	0.18
0.16	0.14	0.12	0.1
0.08	0.06	0.04	0.02

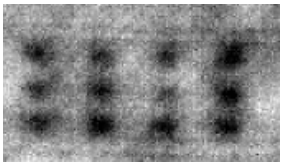

Figure 11 Second derivative at t=1.436s

In the PT and PPT inspection results of the F/A-18 rudders (Figures 12 to 14) a few areas located at the base of the rudders suspected of being delamination were detected. Additionally a few features were also detected and are circled in red in the figures. Structural components such as hinges, metallic reinforcement, filler and skin thickness variations are also visible.

The feature identified as B in Figure 12 is located in an unusual location. Instead of being around the leading edge like most of the other identified features, B is located in the middle of the sandwich structure and is not close to the rudder periphery. A close-up PT inspection of this area was performed and results are shown in Figure 13. The reason for this indication is not known.

* max volume per cell ~0.25ml

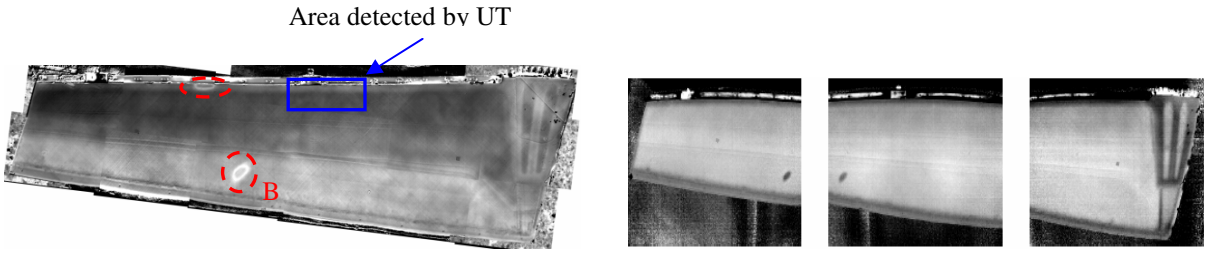

(a) (b)

Figure 12 (a) Second derivative of the pulsed thermography results at 0.367 s. (b) Phase image obtained by PTT at 0.1 Hz. (CF rudder starboard side).

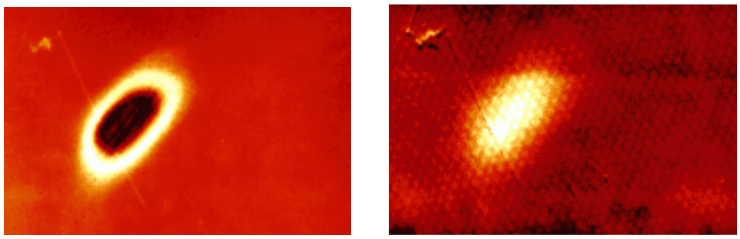

(a) (b)

Figure 13 Raw thermal data of anomaly B at (a) 0.033s and (b) 5.067s.

(a) (b)

Figure 14 (a) Second derivative of the pulsed thermography results at 0.367 s (b) Phase image obtained by PTT at 0.15 Hz. (USN rudder port side).

5.4 Lock in thermography

Figure 15 presents the LT results obtained from the inspection of a reference panel and of a rudder. The phase of the LT thermograms were processed by FFT. As seen, for simulated delaminations and impact damage the results are similar to PT and PPT. However, for simulated disbonds and water ingress the detection of the defective areas varies from barely visible to not visible. LT was not successful in detecting most of the features detected by PT and PPT. It did however clearly show structural information such as metallic reinforcement, filler and skin thickness variations

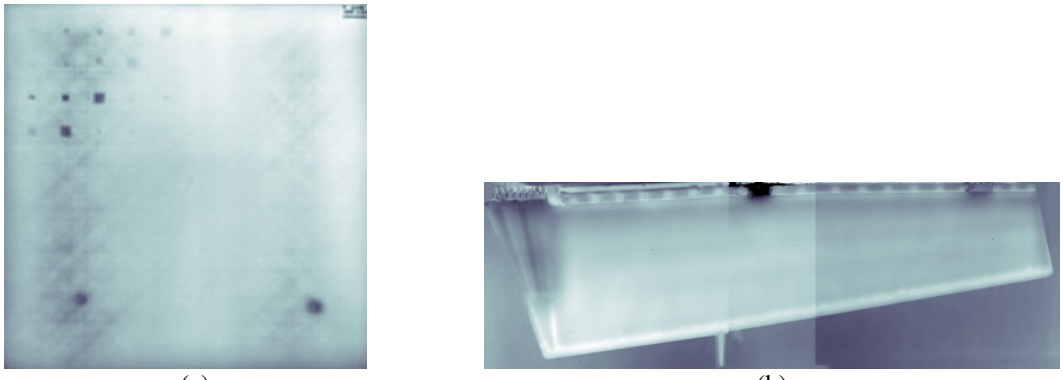

(a) (b)

Figure 15 (a)LT phase image at 0.002Hz of a reference panel. (b)Lock-in thermography phase image at 0.002Hz (CF rudder port side)

5.5 Vibrothermography

5.5.1 Reference panel

The thermograms acquired during VT experiments were processed by FFT. The second amplitude frames focusing on the simulated delamination and disbond areas of a reference panel are presented in Figures 16 and 17. As seen, only inserts number 5, 12, 13 and 17 were detected. These are all larger than 10x10mm. Based on these results, it is believed that the boundary free area must be of a certain minimum size to generate sufficient heat that could be detected under vibration condition. If there is not enough material under free vibration condition, either the heat generated is not sufficient to be detected or no heat is generated since the rubbing and the clapping of the surface under vibration is not adequate.

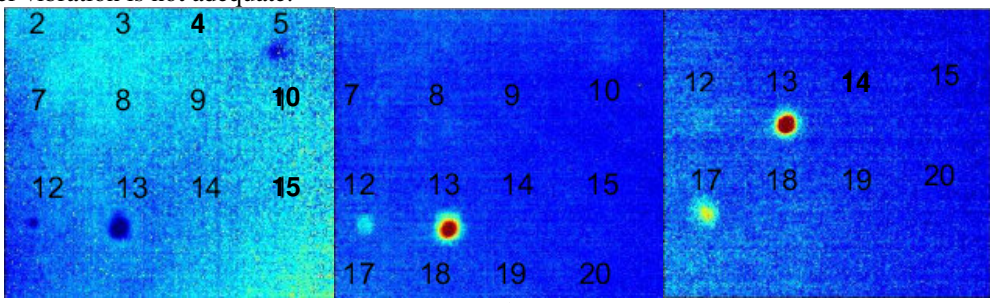

(a) (b) (c)

Figure 16 Vibrothermography inspection results of the area containing simulated delaminations.

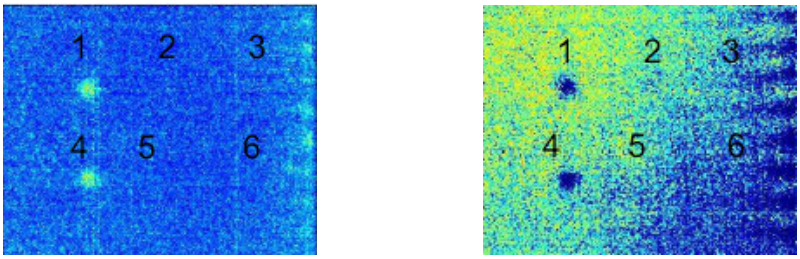

(a) (b)

Figure 17 Vibrothermography inspection results of the area containing simulated disbonds (a) amplitude image; (b) phase image.

Additionally, the simulated node bond failures and the presence of water could not be detected by vibrothermography. The latter one was predictable since water is a coupling agent that transmits vibration. Thus, it does not result in the conversion of mechanical energy into heat. Several reasons could explain the non-detection of the node disbonds: 1) the active surfaces are too small; 2) the excitation frequency used was inadequate; 3) the heat generated was insufficient compared to the skin thickness.

5.5.2 F/A-18 rudders

Due to the physical limitation of the apparatus used, vibrothermography inspections of the rudder were only performed locally. The first inspection performed (Figure 18) focused on the area corresponding to the feature identified by UT inspection and was performed in through transmission mode, i.e. with the ultrasonic welder on the starboard side and the IR camera on the port side. The dots present in the area circled in red are similar to those detected by PT, PPT and LT. After careful visual inspection of the rudder, it appeard that these are bubbles entrapped within the paint layers of the rudder skin.

VT inspections were also carried out on the lower part of the leading edge and results are shown in Figure 19. Delaminations that were also detected with other thermography techniques, as well as two additional features were detected.

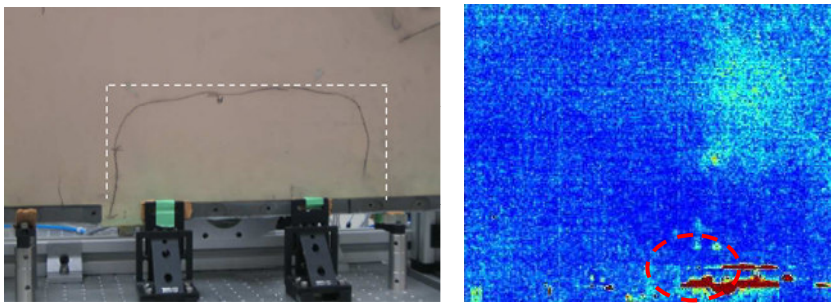

(a) (b)

Figure 18 (a) A photograph of the vibrothermography inspection setup showing the area inspected; (b) phase image obtained by vibrothermography.

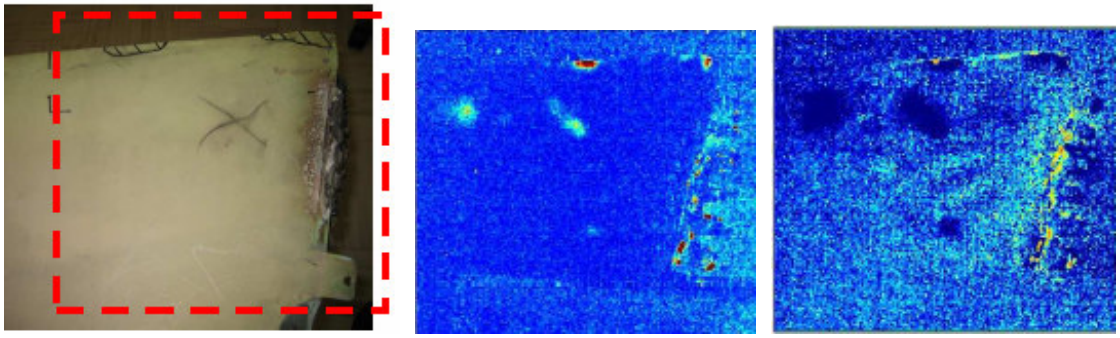

(a) (b) (c)

Figure 19 (a) A photograph of USN rudder port side showing the area inspected; (b) Amplitude image obtained by VT; (c) Phase image obtained by VT;

In Figure 20, features similar to those found on the port side were detected. In addition, streaks usually associated with standing wave were also noticed. This pattern is located at the thinnest section of the rudder. Experiments at different frequencies were conducted to eliminate the standing waves. Nevertheless, the streak features were still detected. Destructive testing did not reveal any particular reason for these features and thus, even though several approaches were taken to avoid standing waves, it is believed that the streak features are the result of standing waves.

After the vibrothermography experiments, USN rudder port side was re-inspected by ultrasound and pulsed thermography (Figure 21) at the NRC-IAR. No indication of additional discontinuities was noticed.

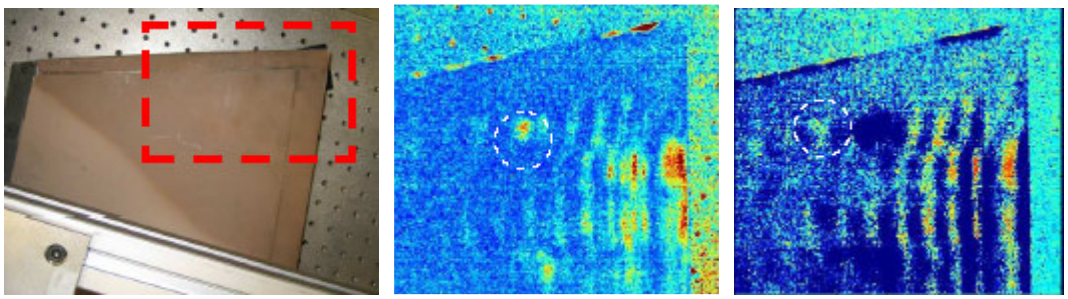

(a) (b) (c)

Figure 20 (a) A photograph of USN rudder port side showing the area inspected; (b) Amplitude image obtained by VT; (c) Phase image obtained by VT;

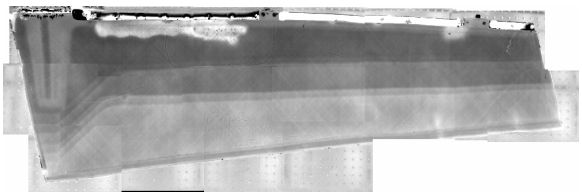

Figure 21 Second derivative of the pulsed thermography results at 0.367 s (port side) – re-inspection after VT.

None of the thermography techniques tried on the reference panels were successful in detecting the simulated node bond failures. This is surprising since rubbing of disbonded nodes should have resulted in heat generation. Moreover, a previous NRC-IAR study has shown that node bond failures can be detected by thermography technique (Figure 22).[7] Therefore, it is believed that the nature of the nodes bond failure and the core material used in the sandwich structure can influence the detectability of the node bond failures.

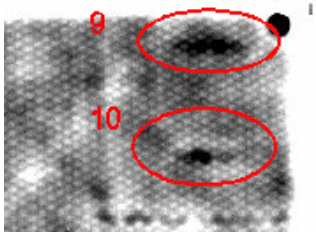

Figure 22 PT result showing node bond failures in honeycomb Nomex® core sandwich structure.[7]

6 Thermography results summary

6.1 PT and PPT

Pulsed thermography provides surface and sub-surface information on large areas of the inspected specimen in an in-situ and fast manner. This is particularly interesting for the inspection of large aerospace components such as rudders. Raw thermal data from a PT experiment is strongly affected by a diversity of problems mainly the following four: (1) non-uniform heating, (2) emissivity variations, (3) background reflections and (4) surface geometry. Nevertheless, different processing techniques are available to deal with these problems. Two of the most powerful processing techniques were considered here: pulsed phase thermography (PPT) and the thermographic signal reconstruction (TSR) combined with derivative processing.

Of all the thermography techniques assessed on the reference honeycomb panels, PT and PPT are the most suitable, in terms of flaw detection and visibility. The visibility of the discontinuities depends on the energy injected into the inspected item and non-uniform heating might affect the results. Results of PT and PPT applied on rudders showed that these techniques are also more sensitive to paint thickness than the other NDE techniques employed. By comparing the PT results of the NRC-IAR (long IR) with those of the UL (mid IR), it can be said that the influence of the IR camera wavelength is negligible.

6.2 LT

Lock-in thermography is an effective technique for the detection of near surface defects. The experimental results, however, indicate that not all defects can be detected with this technique. Results from a reference panel provide some hints on the effectiveness of the technique to inspect anisotropic materials such as CFRP. For instance, the maximal depth attained was around 2.2 mm. Even if the theory is not directly applicable to multi-layers or non-homogenous properties, the results are acceptable.

Results from a reference panel indicate that any honeycomb cell more than half filled with water can be detected with the lock-in method. It is not apparent that a single shot acquisition provides sufficient spatial resolution to detect all defects. Two or three acquisitions provide better results, as spatial resolution increased and energy focused on a smaller area, but this requires an increase in the overall inspection time. The disadvantage of this method is the time needed for the acquisition, which can represent more than one hour for a test at a single frequency. The clear advantage of lock-in thermography is that it can provide the power required to inspect material of low thermal conductivity when the thermal waves have difficulty penetrating deep into the sample. In this study, the LT data obtained on the F/A-18 rudders were inconclusive, and the data provided above is valid for in-lab samples.

6.3 VT

The ultrasound vibrothermography has shown some very interesting defect detection capabilities. First, with simulated delamination and disbond, it can be said that the Teflon inserts can be detected irrespective of their depth location. The planar size of the inserts has an influence on the detection capability, as only the largest inserts (>10x10mm) were detected. This size is below the usual critical flaw size detection requirement, thus it should not be a concern. It is possible that the heat associated with the rubbing of the free moving surfaces is proportional to the free moving surface area, thus limiting the detection capability. The larger the flaw, the greater is the amount of energy that will be converted into heat. The honeycomb core seems to attenuate ultrasonic waves, which limits the VT technique to a reflection method rather than both reflection and through transmission. The influence of the ultrasound injection point is not critical, as long as it is on the same side of the surface inspected. For example, defects located at a distance greater than 400 mm from the injection point were easily detected.

Proper coupling between the sample and the ultrasound booster does not usually leave any marks on the sample surface after the experiment. In this study, water has been used to improve the coupling. Re-inspection using UT and PT showed that no additional damage is done if the coupling pressure is maintained low, typically below 250 PSI.

Water ingress in the honeycomb structure could not be revealed by the ultrasound vibrothermography. In fact, water should not cause any friction in the material so obviously no heat is generated. Instead, water improves the propagation of ultrasound. The same might not be true for frozen water, in which case the ice might vibrate against rudder material and cause friction that might be detected by a sensitive infrared camera. The vibrothermography technique reveals certain anomalies that are due to the non-homogeneity of the material. Even if the material structure is altered, if no friction, clapping or plastic deformation is induced by mechanical excitation, the discontinuities will not generate any heat, thus will not be detected. The effectiveness of this technique relies on the ability of the flaws to react to mechanical waves to cause friction.

7 Conclusion

NDI techniques are generally complementary to each other. No one technique can reveal everything about a specimen. Among all the thermography techniques assessed, PT and PPT seem to provide the results with the highest defect visibility. Nevertheless, VT shows some interesting potential as it detects some features that otherwise can be missed. Unfortunately, the additional features detected by VT could not be correlated with other results and destructive verification tests are needed to establish the nature of the features.

The thermography methods assessed in this paper could be extended to other flight control surfaces made of similar honeycomb sandwich configuration, and similar inspection capabilities should be assumed. Since most of the defects occur between the skin and the core, the thermography techniques should also yield the same capabilities with NOMEX core sandwich panels.

For the detection of water ingress, it has been demonstrated that pulsed thermography can be used and it reduces the aircraft down time by eliminating the need for aircraft cold-soaking. However, the influence of the angle of installed rudders has not been investigated. Nevertheless, PT could be used for detection of water ingress in horizontal flight control surfaces.

All thermography techniques detected the simulated disbonds in the reference panels. However, they failed to reveal the presence of suspected disbonded areas identified by UT in the F/A-18 rudders. Further investigation on the nature of this flaw detected by UT is needed to fully understand the difference between the NDI results. Additionally, more investigation of the features detected by thermography and missed by UT will have to be pursued.

Acknowledgments

This work was partially supported by the Department of National Defence under MOU Annex Number DND/NRC/IAR 2005-10. Mr. Thomas Kay, Mr. Ron Gould, Dr. Chun Li, Mr. Matthieu Harrison, Mr. Thomas Benak, Mr. Brian Moyes, from the NRC-IAR, Capt. Brian Tang, Maj. Vivier Lefebvre and Capt. Leo Post from the Department of National Defence are acknowledged for their sincere assistance and valuable discussions during the course of this work.

References

[1] Canadian Forces Technical Order C-12-188-SRM/ND-000 WP 005/00, dates 1 September 1994.

[2] J.S.R. Giguere, "Damage Mechanisms And Nondestructive Testing in The Case of Water Ingress In CF188 Flight Control Surfaces," DCIEM Technical Memorandum TM 2000-098, August 2000.

[3] Nondestructive Inspection Report On CF188733," USAF Sacramento Air Logistics Center, McClellan AFB, CA, Volumes I and II, March 1996.

[4] http://en.wikipedia.org/wiki/Rudder

[5] McRae, K. I., Bowles, S. J., Lepine, B. A., and Giguere, S., "NDE of Moisture-Related Degradation in Composite Honeycomb Components", Operating Assignment MAT-TP-5-O22: Final Report, TTCP/MAT-TP-5/5/02, November 2002

[6] Lewis, W. J., Bennett, L. G. I., "The Use of Neutron Radiography in the Inspection of Aircraft Composite Flight Control Surfaces", Proceeding of the 1st Pan American Conference for Nondestructive Testing, Toronto, 14-18 September, 1998.

[7] Genest, M., Forsyth, D. S., "Thermographic Inspection of DSTO panels", NRC-IAR Internal Report, LM-SMPL-2005-0003, January 2005.

[8] Genest, M., Forsyth, D. S., "Thermographic Inspection of Rudder U22-162", NRC-IAR Internal Report, LM-SMPL-2005-0065, April 2005.

[9] Canadian Forces, "Thermography Inspection of CF 188 Flight Controls L/H and R/H", Technique #188-316-T, December, 2004.

[10] Maldague, X. P. V., "Theory and Practice of Infrared Technology for Nondestructive Testing", John Wiley & Sons Inc, New York NY, 2001.

[11] Maldague X. and Marinetti S., "Pulse Phase Infrared Thermography", J.Appl. Phys., Vol. 79, pp. 2694-2698, 1996.

[12] Ibarra-Castanedo C. "Quantitative subsurface defect evaluation by pulsed phase thermography: depth retrieval with the phase," *Ph. D. thesis*, Laval University, 2005, http://www.theses.ulaval.ca/2005/23016/23016.pdf

[13] Ibarra-Castanedo, C. and Maldague, X. "Interactive methodology for optimized defect characterization by quantitative pulsed phase thermography," Research in Nondestructive Evaluation, Vol. 16, No. 4, pp1-19, 2005.

[14] Shepard S. M. "Advances in Pulsed Thermography", Andres E. Rozlosnik, Ralph B. Dinwiddie (eds.), Proc. SPIE, Thermosense XXIII, Vol. 4360, pp. 511-515, 2001.

[15] Carslaw, H. S. and Jaeger, J. C., "Conduction of Heat in Solids", 2nd edition, Clarendon Press, Oxford.

[16] Martin R. E., Gyekenyesi A. L., Shepard S. M., "Interpreting the Results, of Pulsed Thermography Data," Materials Evaluation, Vol. 61, No. 5, pp 611-616, 2003.

[17] Shepard, S. M, "Temporal Noise Reduction, compression and Analysis of Thermographic Image Data Sequence", US Patent 6,516,084, February, 2003.

[18] Shepard, S. M., Ahmed, T., Rubadeux, B. A., Wang , D., Lhota, J. R., "Synthetic Processing of Pulsed Thermography Data for Inspection of Turbine Components", Insight Vol.43 No.9, September, 2001.

[19] Busse, G., Wu, D., Karpen, W., "Thermal Wave Imaging With Phase Sensitive Modulated Thermography", J. Appl. Phys. 71, Issue 8, April, 1992.

[20] Perez, I., Forsyth, D. S., Genest, M., "The Effect of Frequency on the Thermosonic Signal", Thermosens XXVI, April, 2004.

[21] Perez, I., Davis, W. R. "Optimizing the thermosonics signal" Review of Progress in QNDE, Vol. 22, pp505-512, 2003.